Proceedings of IWHT2011
2011 International Workshop on Heat Transfer Advances for Energy Conservation and Pollution Control
October 17-20, 2011, Xi'an, China

IWHT2011-053

Normalization of Various Phase Functions and Radiative Transfer Analysis in a Solar Absorber Tube

Brian Hunter, Zhixiong Guo*
Department of Mechanical and Aerospace Engineering
Rutgers, The State University of New Jersey
98 Brett Road, Piscataway NJ, 08854, USA
*Corresponding author: guo@jove.rutgers.edu

ABSTRACT

Phase function normalization is applied to the DOM for predicting radiative heat transfer in a solar absorber tube. Analysis of previous phase function normalization techniques show that while they do conserve scattered energy exactly after DOM discretization, the overall asymmetry factor of the phase function is distorted, leading to changes in scattering effect and errors in heat transfer calculations. An innovative normalization technique which conserves asymmetry factor and scattered energy simultaneously after DOM discretization is applied and compared with the previous technique. The impact of a lack of asymmetry factor conservation is analyzed for both the Legendre polynomial and HG phase function approximations, with larger resulting errors occurring for the HG approximation. The heat flux at the surface of a solar absorber tube, and the energy absorbing rate inside the absorber tube are predicted using the new phase function normalization technique. It is found that the heat fluxes and energy absorption are similar when using the Legendre or the HG approximation with the new normalization technique. Variations of medium optical thickness, scattering albedo, asymmetry factor, and side wall emissivity were scrutinized to determine the effect of said parameters on the wall heat flux and energy absorbing rate inside the solar receiver tube. Side wall heat flux is found to increase with increases in asymmetry factor, optical thickness, and wall emissivity, and with a decrease in scattering albedo. Energy absorbing rate profiles are found to depend greatly on the medium optical thickness and scattering albedo. [**Keywords:** phase function normalization; solar absorber tube; radiative heat transfer; discrete-ordinates method]

INTRODUCTION

For many applications in heat transfer, the contributions of radiation dominate those of conduction and convection. These processes range from determining the thermal efficiency and performance of solar collectors and combustion chambers to the modeling the interaction of laser light with biological tissues [1-5]. When radiation is the dominant mode of heat transfer, accurate and complete solutions of the Equation of Radiative Transfer (ERT) are necessary for full radiation characterization. Many processes, including absorption of solar energy in a solar absorber tube, can be modeled using cylindrical enclosures. In certain cases, heat transfer in cylindrical enclosures can be modeled axisymmetrically, greatly simplifying the solution of the ERT. Many methods have been introduced to numerically solve the ERT, which is an integro-differential equation, and therefore nearly impossible to solve analytically for complex cases. One of the more widely-known solution methods for determining radiative transfer in a medium is the Discrete-Ordinates Method (DOM).

The DOM was introduced by Carlson and Lathrop [6] as an efficient tool to solve the neutron-transport equation, and was later pioneered as a solution technique for the ERT by Fiveland [7-8], where he used the DOM to solve for radiative transfer in rectangular enclosures housing a participating medium. A study by Truelove [9] calculated radiative transfer in a three-dimensional enclosure containing an absorbing-emitting-scattering medium using the DOM, and compared DOM solutions to those determined using the zone method and spherical-harmonics approximation. Use of the DOM for applications involving axisymmetric cylindrical enclosures was presented by Menguc and Viskanta [10], who focused on applying the technique to determine radiative heat flux in furnaces. Jamaluddin and Smith [11] and Jendoubi et al. [12] further implemented the DOM for use in axisymmetric cylindrical enclosures, comparing results for cases with both diffuse and collimated wall incidence. More recently, Guo and Kumar [13,14] extended the use of the DOM to the solution of the time-dependent ERT for use in modeling ultrafast laser applications, such as laser-tissue welding and soldering [15] and laser ablation of cancerous cells from

healthy surrounding biological tissue [16]. A recent publication by Hunter and Guo [17] compared steady-state and transient radiative flux profiles generated with the DOM to those determined using the finite volume method to determine the efficiency and accuracy of each method.

In many participating media, scattering is anisotropic. One major downfall of discretizing the ERT using the DOM is that when scattering is anisotropic, special care must be taken to ensure that scattered energy is exactly conserved. A common technique to guarantee conservation of scattered energy is phase function normalization. By altering the values of the discrete phase function, this constraint is no longer violated. Previous publications have introduced techniques that ensure scattered energy conservation [18,19]. However, Boulet et al. [20] showed that these normalization procedures alter the overall asymmetry factor of the phase function, leading to distinct errors in calculated intensities and fluxes. Recently, to correct this issue, Hunter and Guo [21,22] introduced a new normalization technique that guaranteed exact conservation of scattered energy and phase function asymmetry factor simultaneously after DOM discretization, vastly reducing errors inherent with the old normalization techniques.

The use of solar energy in place of traditional fossil fuels has become a largely researched area recently, due to concerns over pollution and global warming. In solar reactors and power plants, radiant intensity from the sun is absorbed by a solar absorber tube via the use of reflectors and concentrators [23]. The energy absorption is then commonly used to heat a working fluid (such as molten salt [23,24] or thermal oil [25]), which can be used to increase the operating temperature and thermal efficiency of the solar power plant [26]. Solar energy absorption is a key process for many applications, including hydrogen generation [24,27] and production of energy-rich fuels via high-temperature hydrocarbon reformation [28-30]. Jiang et al. [31] investigated the use of beam splitting technology in a concentrated photovoltaic system to reduce the solar heating load on an absorber tube while increasing system efficiency. Wang et al. [25] and Jianfeng et al. [26] determined temperature distributions and heat transfer performance of solar receiver pipes under concentrated solar radiation. Finally, work by Karni et al. [30,32] introduced a novel absorbing material called the “Porcupine”, which can be added to the inner surface of a solar absorber tube to withstand high working temperatures and large solar fluxes in order to increase the thermal efficiency of a solar power plant.

In these solar energy applications, it is essential that heat fluxes and radiative energy absorption are modeled accurately. The radiative processes inside a solar absorber tube can be determined through solution of the ERT with the DOM. However, a lack of conservation of either scattered energy or asymmetry factor could drastically alter numerical results. Thus, for simulation of absorption of solar energy in a solar receiver tube, care must be taken to properly normalize the scattering phase function for accurate numerical predictions.

In this study, the DOM with phase function normalization is used to predict radiative heat transfer in a simplified solar absorber tube. An analysis of the conservation of scattered energy and asymmetry factor are presented for both the Legendre polynomial and Henyey-Greenstein phase function approximations with the different normalization techniques. The impact of a lack of conservation of asymmetry factor on the overall scattering effect, radiative heat flux, and energy absorbing rate inside the solar absorber tube is discussed. Radiative heat fluxes and energy absorption rates inside the solar absorber tube are determined for various asymmetry factors, side wall emissivities, and medium optical thickness and scattering albedo.

NOMENCLATURE

$A^{l'l}$	Normalization parameter
E	Blackbody emissive power [W/m^2]
g	Asymmetry factor
G	Incident radiation [W/m^2]
L	Length of cylindrical enclosure
I	Radiative intensity [W/(m^2·sr)]
M	Total number of angular directions
N	Number of terms in Legendre phase fun.
N_r, N_z	Number of radial and axial control volumes
q	Radiative heat flux [W/m^2]
r	Radial location
R	Radius of cylindrical enclosure
$\hat{\boldsymbol{s}}$	Unit direction vector
w	Discrete direction weight
z	Axial location

Greek Symbols

β	Extinction coefficient, = $\sigma_a + \sigma_s$ [m^{-1}]
ϵ	Emissivity
μ, η, ξ	Direction cosines
Φ	Scattering phase function
$\tilde{\Phi}$	Normalized scattering phase function
ρ	Reflectivity
σ_a	Absorption coefficient [m^{-1}]
σ_s	Scattering coefficient [m^{-1}]
τ	Optical thickness, = βR
Θ	Scattering angle
ω	Scattering albedo, = σ_s/β

Subscripts

b	Blackbody
HG	Henyey-Greenstein scattering
L	Legendre polynomial scattering
med	Medium
w	Boundary wall

Superscripts

$'$	Radiation incident direction
l, l'	Radiation directions
$l'l$	From direction m' into direction m

DISCRETE ORDINATES METHOD

Using the DOM, the steady-state ERT for a gray-diffuse, absorbing-emitting and scattering medium housed in an axisymmetric cylindrical enclosure can be written, for a discrete direction l, as follows [4,5,13,14]

$$\frac{\mu^l}{r}\frac{\partial}{\partial r}[rI^l] - \frac{1}{r}\frac{\partial}{\partial \phi}[\eta^l I^l] + \xi^l \frac{\partial I^l}{\partial z} + \beta I^l = \beta S^l \qquad (1)$$

where μ^l, η^l, and ξ^l are the direction cosines corresponding to the $r, \phi,$ and z directions, respectively. The source term S^l is expressed below, for a discrete direction l:

$$S^l = (1-\omega)I_b + \frac{\omega}{4\pi}\sum_{l'=1}^{M} w^{l'}\Phi^{l'l}I^{l'} \qquad (2)$$

The first term in the preceding equation accounts for blackbody emission of the medium, while the second term accounts for the scattering of radiant energy between two discrete directions l' and l. In the scattering term, $w^{l'}$ is the weighting factor corresponding to the discrete direction l', and $\Phi^{l'l}$ is the discrete scattering phase function between two directions l' and l.

For the considered axisymmetric cylindrical enclosure, the side wall is taken to be a gray-diffuse emitter and reflector. The intensity emanating from a point on the side wall in a discrete direction l can be expressed as

$$I_w^l = \epsilon_w I_{bw} + \frac{\rho_w}{\pi}\sum_{l',\mu^{l'}>0} w^{l'} I^{l'} |\mu^{l'}|, \ \mu^l < 0 \qquad (3)$$

where the two terms account for the emissive power of the wall and the collection of the reflected portions of all incoming intensities, respectively. The end-walls of the cylinder are considered to be purely specular reflectors, and an axisymmetric boundary condition is implemented at the radial centerline. The radiative heat flux at the side wall and incident radiation anywhere in the medium can be calculated using the following summations

$$q_R = \sum_{l=1}^{M} \mu^l w^l I^l \ , \ G = \sum_{l=1}^{M} w^l I^l \qquad (4)$$

The Mie scattering phase function Φ is, in general, a highly oscillatory function. Due to this property, it is extremely difficult to implement the exact Mie function numerically for use in radiative transfer analysis [1,2]. Approximations to the Mie phase function are generally implemented to avoid this issue. Many different techniques for phase function approximation have been presented in literature. One commonly implemented technique is to approximate the Mie phase function using a finite series of Legendre polynomials [1,12,33], as follows:

$$\Phi(\hat{\boldsymbol{s}}', \hat{\boldsymbol{s}}) \approx \Phi_L(\Theta) = \sum_{i=0}^{N} C_i P_i(\cos\Theta) \qquad (5)$$

where Θ is the scattering angle between directions $\hat{\boldsymbol{s}}'$ and $\hat{\boldsymbol{s}}$, and the coefficients C_i are determined from Mie theory. Another widely-used phase function approximation is the Henyey-Greenstein (HG) approximation, which has been used extensively in literature to accurately capture the strong-forward scattering peak for highly anisotropic scattering phase functions [1,2,19]. The analytic form of the HG phase function is

$$\Phi(\hat{\boldsymbol{s}}', \hat{\boldsymbol{s}}) \approx \Phi_{HG}(\Theta) = \frac{1-g^2}{[1+g^2-2g\cos\Theta]^{1.5}} \qquad (6)$$

where g is the phase function asymmetry factor, which is a measure of the average of the cosine of the scattering angle.

In order to ensure scattered energy conservation in the system after DOM discretization, the discrete scattering phase function $\Phi^{l'l}$ must satisfy the following conservation condition, for a given direction l'

$$\frac{1}{4\pi}\sum_{l=1}^{M} \Phi^{l'l} w^l = 1 \qquad (7)$$

The discrete scattering phase function $\Phi^{l'l}$ between directions l' and l can be expressed, using the Legendre polynomial phase function approximation of Eq. (5), as follows for an axisymmetric cylindrical medium

$$\Phi^{l'l} = \frac{1}{2}[\Phi_L(\Theta_1) + \Phi_L(\Theta_2)] \qquad (8)$$

where the cosines of the scattering angles Θ_1 and Θ_2 are calculated using the following expressions

$$\begin{aligned} \cos\Theta_1 &= \mu^l\mu^{l'} + \eta^l\eta^{l'} + \xi^l\xi^{l'} \\ \cos\Theta_2 &= \mu^l\mu^{l'} - \eta^l\eta^{l'} + \xi^l\xi^{l'} \end{aligned} \qquad (9)$$

The preceding equations are also valid if the HG phase function approximation is instead implemented. The necessity of using two scattering angles comes from the axisymmetric nature of the problem, in which the discrete ordinate η is determined from the discrete ordinates μ and ξ using the relationship $\eta = \pm\sqrt{1-\mu^2-\xi^2}$. The square root operator leads to two possible signs for each discrete ordinate η, leading to the sign difference between the expressions for each scattering angle in Eq. (9).

In addition to satisfying the scattered energy conservation relation of Eq. (7), the discrete scattering phase function should also satisfy the following constraint to ensure that the phase function asymmetry factor g is conserved after DOM discretization:

$$\frac{1}{4\pi g}\sum_{l=1}^{M}\Phi^{l'l}\cos(\Theta^{l'l})\,w^{l}=1 \qquad (10)$$

Taking into consideration the two possible signs of η once more, the product $\Phi^{l'l}\cos(\Theta^{l'l})$ can be expressed using an average of phase functions calculated at each individual scattering angle:

$$\Phi^{l'l}\cos\left(\Theta^{l'l}\right)=\frac{1}{2}[\Phi_L(\Theta_1)\cos\,\Theta_1+\Phi_L(\Theta_2)\cos\,\Theta_2] \qquad (11)$$

Once again, Eqs. (10-11) are also valid for the HG phase function approximation. Both the scattered energy conservation constraint of Eq. (7) and the asymmetry factor conservation constraint of Eq. (10) should be explicitly satisfied after DOM discretization in order to ensure that the solution of the ERT is accurate [21,22]. However, for cases where scattering is highly anisotropic, further care must be taken to ensure that these conservation constraints are attained. Further details on the discretization and solution of the ERT using the DOM are not presented here, for brevity, but can be referenced from textbooks [1,2] and journal publications [3-5,13-17].

PHASE FUNCTION NORMALIZATION

Figs. 1(a-b) show the seven Legendre polynomial phase function approximations that are considered in this study. The expansion coefficients for the three functions in Fig. 1(a) are presented by Kim and Lee [33], while the expansion coefficients for the four phase functions in Fig. 1(b) are given by Lee and Buckius [34].

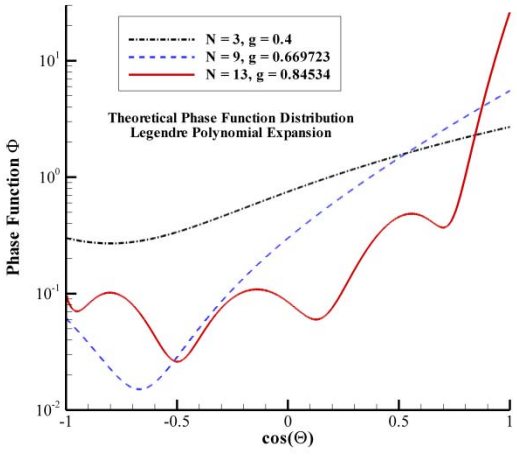

(a)

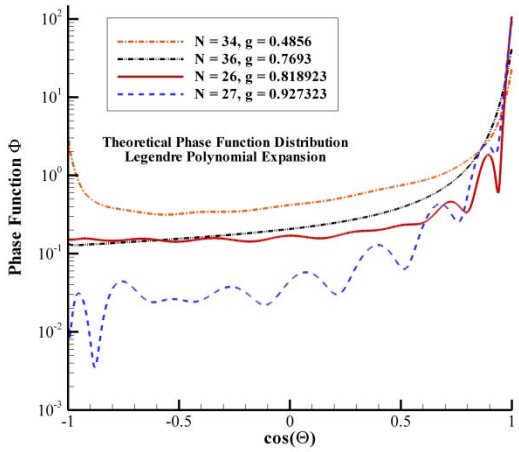

(b)

Figure 1: Legendre polynomial phase function approximations

The seven Legendre polynomial phase functions are defined by their asymmetry factors and the number of terms used in the polynomial expansion, as seen in Figs. 1(a-b). For comparison purposes, HG phase functions with the same asymmetry factors as the seven functions presented below are also analyzed in this study to gauge the effectiveness of using each approximation.

As previously mentioned, as scattering becomes highly anisotropic, the scattered energy and asymmetry factor conservation constraints are not always satisfied. Table 1 shows the minimum and maximum values of the scattered energy conservation constraint of Eq. (7) after DOM discretization using both the Legendre polynomial and HG phase function approximations. The values were obtained using the DOM S16 (288 total discrete ordinates) quadrature. For scattered energy to be exactly conserved, the minimum and maximum values of the summation in Eq. (7) should both be unity.

Table 1: Examination of conservation of scattered energy for various asymmetry factors

Scattered Energy Conservation Condition Values			
		Legendre	HG
g (Prescribed)	N	Minimum/Maximum	Minimum/Maximum
0.4	3	1.0/1.0	1.0/1.0
0.4856	34	0.976/1.028	0.998/1.003
0.669723	9	0.999/1.001	0.989/1.014
0.7693	36	0.958/1.050	0.974/1.043
0.818923	26	0.932/1.132	0.970/1.104
0.84534	13	0.974/1.027	0.981/1.184
0.927323	27	0.894/1.091	1.269/2.825

For g = 0.4, scattered energy is effectively conserved when both the Legendre polynomial and HG phase function approximations are implemented. However, as asymmetry

factor increases, deviations from unity appear. For the HG phase function, an increase in asymmetry factor produces a strict decrease in minimum summation value and a strict increase in maximum summation value until g = 0.84534. At this value, the minimum starts to increase along with the maximum, and at g = 0.927323 both values start to diverge. A similar linear correlation with asymmetry factor is not seen for the Legendre polynomial approximation. While the minimum and maximum do deviate from unity as asymmetry factor increases, there is also a dependence on the number of terms in the Legendre expansion. The three functions in Fig. 1(a) produce much smaller deviations from unity than the four functions in Fig. 1(b). For example, for the N = 9 expansion (g = 0.669723), scattered energy is almost exactly conserved, with the minimum and maximum value of the summation reaching 0.999 and 1.001, respectively. Conversely, for the N = 34 expansion (g = 0.4856), the minimum and maximum are 0.976 and 1.028, respectively, which differs from the pattern witnessed with the HG approximation. This indicates that both the asymmetry factor and the number of terms/actual shape of the Legendre polynomial expansion have an impact on the conservation of scattered energy after DOM discretization.

In order to ensure the exact conservation of scattered energy in the system, the scattering phase function must be normalized. Previous publications have introduced normalization techniques that guarantee the satisfaction of Eq. (7). The most widely-used and well-known technique, introduced by Kim and Lee [18], is to normalize the scattering phase function in the following manner

$$\tilde{\Phi}^{l'l} = \Phi^{l'l} * \left(\frac{1}{4\pi} \sum_{l=1}^{M} \Phi^{l'l} w^{l} \right)^{-1} \tag{12}$$

The multiplication of each discrete phase function value by the inverse of the conservation condition guarantees that Eq. (7) will be satisfied. A second technique, pioneered by Wiscombe [19], introduces corrective factors for each individual direction to normalize the scattering phase function, as follows:

$$\tilde{\Phi}^{l'l} = \left(1 + \gamma^{l} + \gamma^{l'}\right) \Phi^{l'l} \tag{13}$$

where the corrective factors γ^{l} and $\gamma^{l'}$ are solutions to the following system of equations

$$\frac{1}{4\pi} \sum_{l=1}^{M} (1 + \gamma^{l} + \gamma^{l'}) \, \Phi^{l'l} w^{l} = 1 \ , \ \ l' = 1,2, \dots, M \tag{14}$$

Both procedures are structured so that scattered energy is explicitly conserved. However, while scattered energy is conserved using the previous techniques, work by Boulet et al. [20] and Hunter and Guo [21] showed that these techniques do not ensure the conservation of asymmetry factor, i.e. Eq. (10) is not exactly conserved after normalization. The deviation in overall asymmetry factor after discretization can lead to errors in resulting intensity fields and flux profiles.

To address this issue, Hunter and Guo [21,22] introduced a new phase function normalization technique, which guarantees exact conservation of both scattered energy and asymmetry factor simultaneously. The phase function is normalized in the following way:

$$\tilde{\Phi}^{l'l} = (1 + A^{l'l}) \Phi^{l'l} \tag{15}$$

where the normalization parameter $A^{l'l}$ corresponds to scattering between two discrete directions l' and l. The normalized scattering phase function $\tilde{\Phi}^{l'l}$ is subject to the following constraints:

$$\frac{1}{4\pi} \sum_{l=1}^{M} \tilde{\Phi}^{l'l} w^{l} = 1, \qquad l' = 1,2, \dots, M \tag{16a}$$

$$\frac{1}{4\pi g} \sum_{l=1}^{M} \tilde{\Phi}^{l'l} \cos\left(\Theta^{l'l}\right) w^{l} = 1, \qquad l' = 1,2, \dots, M \tag{16b}$$

$$\tilde{\Phi}_{l'l} = \tilde{\Phi}_{ll'} \tag{16c}$$

The first two constraints are the conservation constraints of Eq. (7) and Eq. (10), and the third constraint is a symmetry condition. The system 16(a-c) has more unknowns ($(M^2 + M)/2$) than equations ($2M$), and thus has infinite solutions. The desired normalization parameters that exactly satisfy conservation of scattered energy and phase function asymmetry factor are determined by calculating the minimum-norm solution of the system 16(a-c) using QR decomposition [35].

The importance of conservation of asymmetry factor can be seen in Table 2. According to the isotropic scaling law [36,37], the reduced scattering coefficient is expressed as $(1 - g)\sigma_s$, and the change in overall scattering effect due to the lack of conservation in asymmetry factor can be determined by comparing values of $(1 - g)$ before and after DOM discretization. Table 2 shows both the overall asymmetry factor and change in scattering effect after discretization when normalization is ignored, as well as when both the old technique of Eq. (12) and Hunter and Guo's technique are implemented. Results for both the Legendre polynomial and HG phase function approximations are presented.

For g = 0.4, asymmetry factor is exactly conserved after discretization for both phase function approximations without normalization, indicating that further normalization is unnecessary. As asymmetry factor increases, discrepancies in the discretized asymmetry factor start to appear. For the HG phase function, the percent difference in scattering effect when normalization is ignored increases drastically as asymmetry factor increases, ranging from 0.102% at g = 0.4856 to 1053.947% at g = 0.927323. For the Legendre approximation, an increase in asymmetry factor from g = 0.4 produces an increase in change in scattering effect. However, as was the case for the scattered energy condition, the phase functions in Fig. 1(a) show a smaller change in scattering effect than do the phase functions in Fig. 1(b) after discretization.

For example, the change in scattering effect when normalization is ignored for the N = 13 phase function (g = 0.84534) is 2.095%. However, for the N = 26 expansion (which has a lower asymmetry factor g = 0.818923), the change in scattering effect is 11.916%. These results further the notion that the number of terms and physical shape of the Legendre approximation, as well as the asymmetry factor, have an effect on the conservation of both scattered energy and asymmetry factor after DOM discretization.

Table 2: Comparison of asymmetry factor and scattering effect after DOM discretization

		Legendre / HG		
g (Prescribed)	**Normalization**	**N (Leg.)**	**g**	**% Diff (1-g)**
0.4	None	3	0.4/0.4	**0.00/0.00**
	Old		0.4/0.4	**0.00/0.00**
	New		0.4/0.4	**0.00/0.00**
0.485623	None	34	0.4871/0.4851	**0.287/0.102**
	Old		0.4862/0.4853	**0.112/0.063**
	New		0.485623/0.485623	**0.00/0.00**
0.669723	None	9	0.6693/0.6687	**0.128/0.310**
	Old		0.6695/0.6694	**0.068/0.097**
	New		0.669723/0.669723	**0.00/0.00**
0.7693	None	36	0.7729/0.7740	**1.560/2.037**
	Old		0.7702/0.7704	**0.390/0.477**
	New		0.7693/0.7693	**0.00/0.00**
0.818923	None	26	0.8405/0.8426	**11.916/13.076**
	Old		0.8234/0.8232	**2.472/2.362**
	New		0.818923/0.818923	**0.00/0.00**
0.84534	None	13	0.8421/0.8973	**2.095/33.596**
	Old		0.8449/0.8530	**0.284/4.953**
	New		0.84534/0.84534	**0.00/0.00**
0.927323	None	27	0.9356/1.6933	**11.389/1053.947**
	Old		0.9287/0.9576	**1.895/41.660**
	New		0.927323/0.927323	**0.00/0.00**

When the old normalization technique is implemented, the differences in scattering effect are drastically reduced, but are still noticeable, especially for high asymmetry factors. For the HG approximation, the percent changes in scattering effect are 2.362%, 4.953% and 41.660% for g = 0.818923, 0.84534 and 0.927323, respectively. For the Legendre approximation, the percent changes in scattering effect are 2.472%, 0.284% and 1.895% for the same prescribed asymmetry factors. These discrepancies, although much smaller than without phase function normalization, can still produce significant deviations in the physical results. When the new normalization technique is implemented, asymmetry factor is exactly conserved, leading to no change in scattering effect for either approximation.

Table 3 lists the average percent difference from the theoretical phase function values of the discretized phase function values computed with both old and new normalization for the seven considered phase functions. For both HG and Legendre polynomial phase functions, significant discrepancies from the theoretical phase function start to appear for highly anisotropic scattering when the old normalization technique is implemented. Once again, for the Legendre approximation, the number of terms/phase function shape has an impact on the discretized values. The phase functions in Fig. 1(a) (g = 0.4, 0.669723, 0.84534) produce average percent differences of 0.0197%, 0.0795%, and 1.4736%, respectively, when the old normalization is implemented. The expressions in Fig. 1(b) (g = 0.485623, 0.7693, 0.818923, 0.927323) produce larger average percent differences of 1.2430%, 2.1943%, 6.0073% and 5.0106%, respectively. We can see that, in general, increases in asymmetry factor for each grouping produce increases in the difference from theoretical, but once again, the Legendre phase functions generated with fewer terms differ less from theoretical than those with larger numbers of terms. Interestingly, the 27-term g = 0.927323 phase function predicts closer to theoretical than does the 26-term g = 0.818923 phase function. This result could stem from the specific shapes of the phase functions. Looking at Fig. 1(b), the g = 0.818923 approximation shows small oscillations for small scattering cosine, but then large oscillatory action and a sharp peak for high scattering cosine. The g = 0.927323 phase function has more pronounced oscillations, but the increase in phase function value is more gradual overall. The sharp oscillations and peak in the g = 0.818923 phase function could lead to the larger average difference from the theoretical phase function values.

Table 3: Average percent difference from theoretical phase function values of Legendre and HG phase function approximations with old and new normalization

DOM Discretized Legendre Phase Function					
	Avg % Diff. from Theoretical Phase Function				
		Legendre		HG	
g (Prescribed)	**N**	**Old Norm.**	**New Norm.**	**Old Norm.**	**New Norm.**
0.4	3	0.0197	0.0197	0.0649	0.1428
0.485623	34	1.2430	0.5224	0.1374	0.2422
0.669723	9	0.3142	0.0795	0.6584	0.5097
0.7693	36	2.1943	0.5716	1.7647	0.6089
0.818923	26	6.0073	1.7150	3.4545	0.6634
0.84534	13	1.4736	0.9006	5.2664	0.8239
0.927323	27	5.0108	1.4657	40.6550	2.3213

For the HG phase function approximation, a strict increase in average percent difference from the theoretical phase function values is seen as asymmetry factor increases. For highly anisotropic scattering, this difference reaches 40.65% for g = 0.927323. For both phase function approximations, the new normalization technique results in a noticeable decrease in average percentage difference from theoretical for high asymmetry factors. For example, for g = 0.927323, the percent difference decreases from 5.0108% to 1.4657% when new normalization is used with the Legendre polynomial phase function, and from 40.655% to 2.3213% when the new normalization is implemented with the HG phase function.

To further clarify the data in Table 3 and the discussion above, Figs 2(a-b) plot the discretized phase function values

calculated with both old and new normalization techniques for g = 0.927323. The theoretical phase function distribution is included for comparison purposes. The phase functions are plotted versus the cosine of Θ_1 (the first scattering angle in Eq. (9)), and the necessity of using two scattering angles described above leads to the oscillatory behavior of the theoretical phase function. For the Legendre polynomial expansion in Fig. 2(a), both normalization procedures conform fairly accurately to the theoretical values, with only a slightly noticeable discrepancy appearing for the old normalization technique. However, for the HG phase function in Fig. 2(b), an extreme discrepancy can be seen between the old and new normalization techniques. The old normalization produces a phase function profile that is drastically shifted from the theoretical, due to the fact that the asymmetry factor is altered from g = 0.927323 to g = 0.9575. These results for the HG phase function match results presented by Boulet et al. [20] and Hunter and Guo [21]. When the new normalization technique is considered, the discretized values match closely to the theoretical phase function. The above results mandate the necessity for ensuring the conservation of both scattered energy and asymmetry factor after DOM discretization, regardless of phase function approximation.

PHYSICAL RESULTS AND DISCUSSION

The computing workstation used for the results in this analysis is a Dell Optiplex 780, with an Intel 2 Dual Core 3.16 GHz processor and 4.0 GB of RAM. The DOM procedure was implemented using the FORTRAN computing language, and the values of the normalization parameters were determined by using MATLAB, and imported into FORTRAN. Since the normalization parameters depend solely on the quadrature scheme and phase function asymmetry factor, and not on the physical properties of the problem, they need only be determined once for a given phase function.

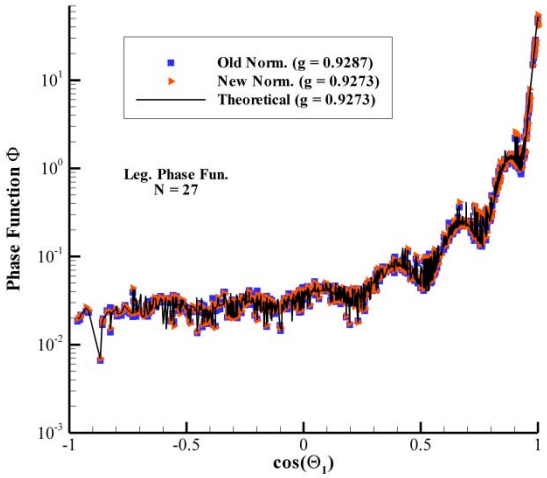

(a)

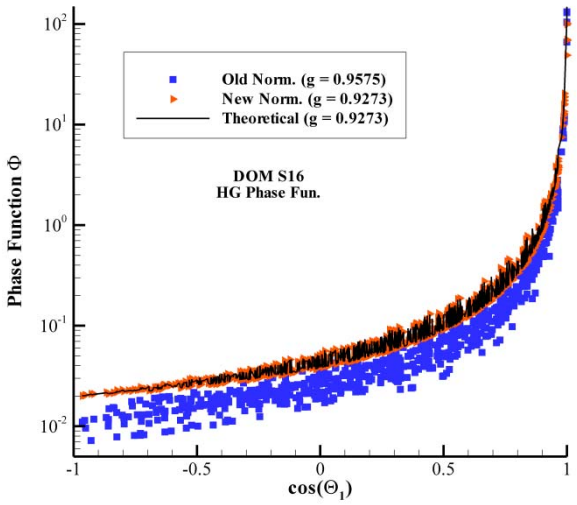

(b)

Figure 2: DOM discretized phase function values vs. cosine of scattering angle with old and new normalization for a) Legendre polynomial and b) HG phase function approximations

The test problem for this study involves the simple modeling of an absorber tube in a solar energy power plant. In most solar power plants, a working fluid passes through an absorber tube, where radiant energy from the sun is absorbed and transferred into the working fluid for later use.

Commonly, absorbing and scattering materials are added to the inside of the absorber tube in order to enhance the absorption of solar energy and increase the total energy transferred to the working fluid. Some common examples of materials used for this purpose are alumina-silica [30,32] and other various porous ceramic materials.

For this study, an axisymmetric cylindrical enclosure containing a homogeneous participating medium is analyzed. The enclosure has radius R and length L. The end walls of the absorber tube are taken as mirrors, to account for the neglecting of end effect because a real absorber tube is quite long. The use of mirror end walls also means that heat flux profiles will be constant along the length of the cylinder, so changes in absorber tube aspect ratio can be neglected. The spatial grid considered was $(N_r \times N_z) = 40 \times 40$ for all simulations. The high radiant heating from the sun is approximated as a diffuse boundary condition on the side wall of the enclosure, with surface temperature 1000 K. The wall of the absorber tube is usually metallic and thin, so that heat loss due to conduction through the wall is negligible. The participating medium housed inside the absorber tube has optical thickness τ and scattering albedo ω, and the inner surface of the side wall is taken to have emissivity ϵ_w. These properties are later varied to gauge the effect of different material properties on the absorption of solar energy. Finally,

the medium is assumed to be cold throughout ($I_b = 0$) to demonstrate solar radiative heat transfer only.

Normalization and Phase Function Approximation Impact

In the previous section, the effect of both old and new normalization on conservation of scattered energy and asymmetry factor was examined for the Legendre polynomial and HG phase function approximations. It is beneficial, however, to examine the effect of the normalization techniques on physical results, such as the absorber tube side wall heat flux, in order to further validate the absolute necessity of conserving both scattered energy and asymmetry factor. Table 4 lists the percentage difference of side wall heat flux between different combinations of phase function approximations and normalization for the seven considered phase functions. The heat flux is non-dimensionalized by the side wall emissive power. The difference in heat flux when old and new normalization is implemented is compared for both the Legendre and HG approximation. Furthermore, a comparison of the heat flux calculated with the HG with new normalization and the Legendre with new normalization is also presented. To analyze the heat flux, the material properties and emissivity of the side wall were held constant ($\tau = 10, \omega = 0.92, \epsilon_w = 0.99$).

Table 4: Comparisons of non-dimensional side wall heat flux

Percent Difference Comparison of $q^*(R,z)$				
τ = 10.0, ω = 0.92, ϵ = 0.99				
g	N	Leg. Old to Leg. New	HG Old to HG New	HG New to Leg. New
0.4	3	0.0000	0.0033	0.0189
0.485623	34	0.0826	0.0039	0.1355
0.669723	9	0.0105	0.0176	0.0758
0.7693	36	0.1511	0.1525	0.0631
0.818923	26	0.4788	0.4371	0.0302
0.84534	13	0.0219	0.7503	0.0387
0.927323	27	0.2187	2.6343	0.0139

When comparing the Legendre approximation with old and new normalization, we see that the percentage differences in heat flux are extremely small. The maximum difference occurs for g = 0.818923, and is less than 0.5%. Once again, slightly larger percent differences are seen for the four phase functions in Fig. 1(b) as compared to the three in Fig. 1(a). When comparing the old and new normalized HG phase function heat fluxes, a strict increase is again seen as asymmetry factor increases, with the difference reaching 2.6343% for g = 0.927323. When the heat fluxes calculated with the HG and Legendre with new normalization are compared, we see that the percentage difference is less than 0.15% for all asymmetry factors, leading to the conclusion that the choice of phase function approximation has little to no effect on the wall heat flux. In general, the differences in heat flux when old and new normalizations are implemented is small, due to the magnitude of the heat flux stemming from the high emissive power of the wall.

In addition to comparing the heat flux leaving the side wall, a comparison of the amount of radiant energy absorbed by the participating medium is also performed for both phase function approximations with old and new normalization. This comparison is of particular importance for the solar absorber, as the energy absorption directly is transferred to the working fluid in order to power the other processes in the solar power plant. The volumetric radiative energy absorption rate, or the amount of energy that is absorbed by the participating medium, is expressed as

$$g_{rad} = \beta(1-\omega)(G - 4\pi I_b) \tag{16}$$

For the case studied (where the medium is cold), $I_b = 0$. The volumetric radiative energy absorption rate can be non-dimensionalized by the wall emissive power and absorber tube radius, in the following manner

$$g^*_{rad} = \frac{\beta(1-\omega)(G)}{\frac{4\pi I_b}{R}} = \tau(1-\omega)G^* \tag{17}$$

Table 5 lists the maximum percentage difference of non-dimensonalized volumetric radiative energy absorption rate along the absorber tube radius between the same combinations of phase function approximation and normalization technique as previously shown in Table 4.

Table 5: Comparisons of non-dimensional volumetric radiative energy absorption rate along the absorber tube radius

Maximum Percent Difference Comparison of $g^*_{rad}(r,H)$				
τ = 10.0, ω = 0.92, ϵ = 0.99				
g	N	Leg. Old to Leg. New	HG Old to HG New	HG New to Leg. New
0.4	3	0.0000	0.0147	0.3978
0.485623	34	0.5109	0.0335	1.5581
0.669723	9	0.0247	0.1905	0.8785
0.7693	36	0.8759	0.8281	0.3323
0.818923	26	2.7807	2.0798	0.4822
0.84534	13	0.2129	3.4211	0.2243
0.927323	27	0.9362	9.7318	0.2190

The data indicates that normalization technique has a larger impact on the energy absorption rate than on the heat flux. When comparing the Legendre approximation with old and new normalization, the largest difference is 2.7807% for g = 0.818923. The previously seen pattern between the phase functions in Figs. 1(a) and 1(b) is again witnessed. When the HG approximation is used, much larger differences in energy absorption rate occur for highly anisotropic scattering, with the percentage difference reaching a maximum of 9.7318% at g = 0.927323. These larger differences result from the lack of conservation of asymmetry factor, and mandate the necessity of exact conservation. When comparing the HG to the Legendre with the new normalization technique, differences are less than 1% for all asymmetry factors except g = 0.485623. The larger difference of 1.5581% could stem from the backward scattering lobe of the Legendre phase function, as the HG phase function for the same asymmetry factor does not contain this

lobe. In general, however, the excellent correlation between results calculated with both the HG and Legendre approximations with new normalization indicate that the two approximations can be implemented interchangeably without distinct consequences.

Solar Absorber Parametric Study

As previously mentioned, there are various materials that can be added to the inside of a solar absorber tube to enhance the absorption of radiant energy. A parametric study was performed to gauge the impact of different material properties and side wall emissivity on both the heat flux leaving the side wall and the volumetric radiative energy absorption rate along the absorber tube radius. In the previous section, it was determined that as long as the new normalization technique is implemented, the Legendre and HG approximations can be used interchangeably. For this parametric study, the Legendre polynomial approximation was implemented with the new normalization technique introduced by Hunter and Guo.

Fig. (3) examines the change of volumetric radiative energy absorption rate versus radial location for changes in asymmetry factor. The medium was taken to have optical thickness $\boldsymbol{\tau = 10}$, scattering albedo $\boldsymbol{\omega = 0.92}$, and the side wall emissivity was taken to be $\boldsymbol{\epsilon_w = 0.99}$.

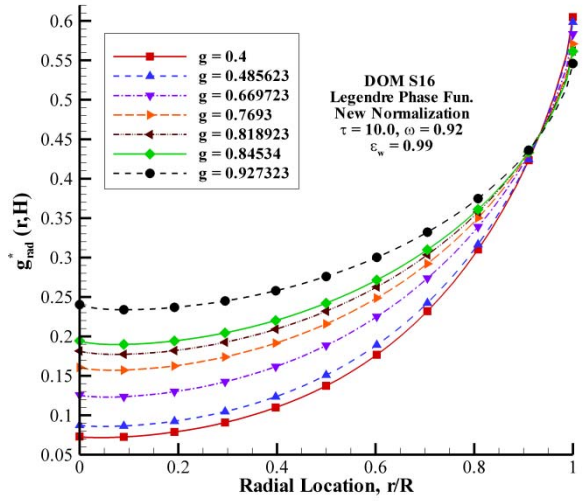

Figure 3: Volumetric radiative energy absorption rate vs. radial location with varying asymmetry factor

Far away from the side wall, the amount of energy absorbed by the medium increases as asymmetry factor increases. This is due to the fact that as scattering becomes more highly anisotropic, the radiant energy is more strongly scattered away from the side wall, leading to higher intensity values near the radial centerline and lower intensity values near the side wall. This explains the opposite trend near the side wall, where the largest volumetric radiative energy absorption rate occurs for $g = 0.4$, and the smallest for $g = 0.927323$.

Fig. (4) plots the variations of side wall heat flux versus phase function asymmetry factor for varying medium optical thickness. The scattering albedo and wall emissivity are kept fixed at $\boldsymbol{\omega = 0.92}$ and $\boldsymbol{\epsilon_w = 0.99}$. The values of optical thickness that were examined ranged from $\boldsymbol{\tau = 1}$ to $\boldsymbol{\tau = 100}$.

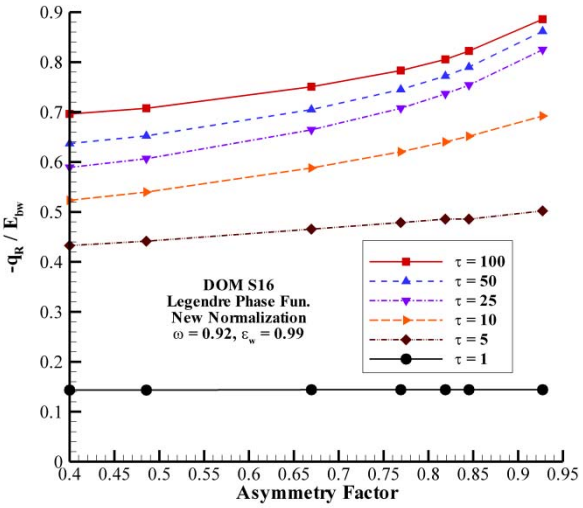

Figure 4: Side wall heat flux vs. asymmetry factor for varying optical thickness

For all asymmetry factors, the non-dimensional heat flux emanating from the side wall increases in magnitude as the optical thickness increases, since more radiant energy can be captured by the medium. The increase in heat flux as optical thickness increases is more pronounced for larger asymmetry factors. For example, the heat flux ratio between the extremely thick medium ($\tau = 100$) and the thin medium ($\tau = 1$) is 4.86 for $g = 0.4$, 5.44 for $g = 0.7693$, and 6.15 for $g = 0.927323$.

Additionally, for all optical thicknesses, side wall heat flux increases with increasing asymmetry factor. For $\tau = 1$, the increase is minimal, with the difference in heat flux between $g = 0.927323$ and $g = 0.4$ only reaching 0.64%. The small difference in heat flux is due to the fact that the radiant energy propagates quickly through the optically thin medium, so the increase in degree of forward scattering is negligible. As optical thickness increases, the difference in heat fluxes determined for various asymmetry factors becomes noticeable. The difference between heat fluxes calculated with $g = 0.927323$ and $g = 0.4$ attains a maximum of 40.07% for $\tau = 25$. As optical thickness increases further, the effect of asymmetry factor becomes less significant, with the percent difference of heat flux calculated at these two asymmetry factors decreasing to 27.26% for $\tau = 100$.

Fig. (5) plots the volumetric radiative energy absorption rate versus radial location for various optical thicknesses with $g = 0.927323$. Near the side wall, increases in optical

thickness produce increases in energy absorption rate, similar to the results for heat flux seen in Fig. (4). For optical thickness less than $\tau = 10$, radiant energy is able to propagate strongly throughout the entire medium, leading to flatter radial energy absorption rate profiles. However, for extreme optical thicknesses, the propagation distance of the radiant energy drastically decreases, leading to sharp drops in the energy absorption rate as one moves from the side wall to the radial centerline. For example, the energy absorption rate at the side wall is only 1.05 times greater than at the radial centerline for $\tau = 1$. Conversely, for the extremely thick medium with $\tau = 100$, the energy absorption rate at the side wall is five orders of magnitude higher than at the radial centerline. The inlay in Fig. (5) more clearly shows the behavior of the energy absorption rate close to the radial centerline. For $\tau = 25$ and greater, the lack of radiant energy propagation causes a decrease in energy absorption rate at the radial centerline as compared with results for the thinner media.

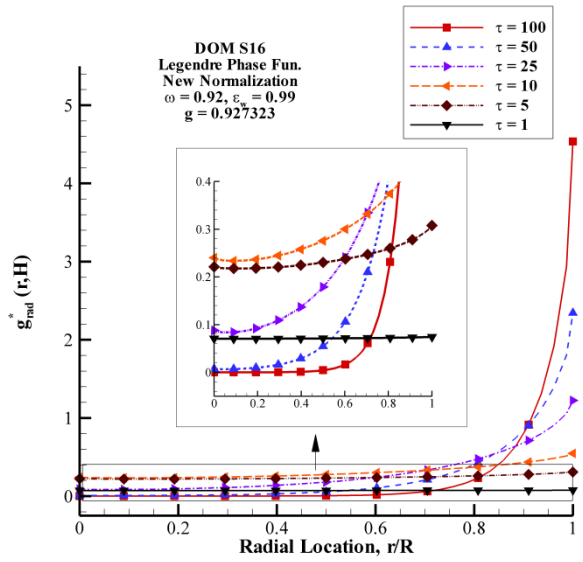

Figure 5: Volumetric radiative energy absorption rate vs. radial location for various optical thicknesses with g = 0.927323

Fig. (6) examines side wall heat flux versus phase function asymmetry factor for varying values of medium scattering albedo. The scattering albedo was varied from $\omega = 0.98$, where nearly all particle extinction is caused by scattering, to $\omega = 0.68$, where absorption has a significant effect on particle extinction. The optical thickness and wall emissivity are kept constant at $\tau = 10$ and $\epsilon_w = 0.99$. As scattering albedo decreases, the magnitude of the heat flux emanating from the side wall increases due to the ability of the medium to absorb more radiant energy. In contrast to the results shown for variations in optical thickness, the increase in heat flux with change in scattering albedo is more pronounced for smaller asymmetry factors. The ratio of heat fluxes calculated with $\omega = 0.68$ and $\omega = 0.98$ is 22.3 for $g = 0.4$, 21.1 for $g = 0.7693$, and 20.5 for $g = 0.927323$.

Heat flux away from the wall again increases as asymmetry factor increases, as expected. For $\omega = 0.68$, the heat flux for $g = 0.4$ is 14.8% lower than for $g = 0.927323$. The percent difference of heat flux between these two asymmetry factors tends to increase as scattering albedo increases, reaching a maximum of 32.3% for $\omega = 0.92$. For $\omega = 0.98$, where the effect of absorption is far outweighed by scattering, the effect of asymmetry factor starts to become less significant, with the difference in heat flux between the two asymmetry factors decreasing to 21.4%.

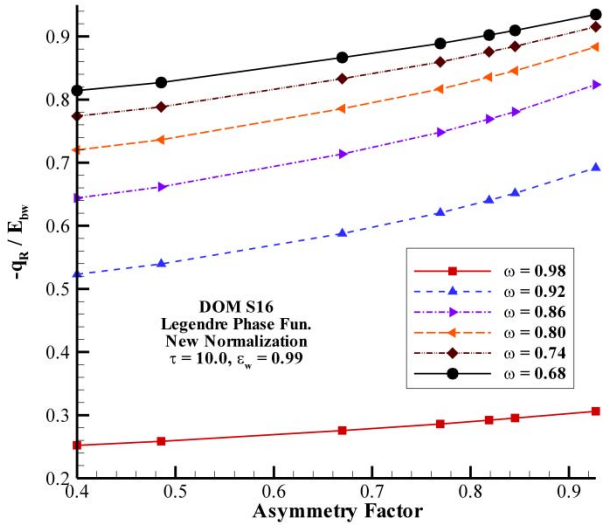

Figure 6: Side wall heat flux vs. asymmetry factor for various scattering albedos

Variations of volumetric radiative energy absorption rate with changes in scattering albedo are examined in Figs. 7(a-b). The medium analyzed in Fig. 7(a) has optical thickness $\tau = 1$, while the medium analyzed in Fig. 7(b) has optical thickness $\tau = 10$. For the thin medium in Fig. 7(a), we see that increases in scattering albedo produce decreases in energy absorption rate for all radial locations. For $\omega = 0.98$, the energy absorption rate is nearly constant for all radial locations, with the energy absorption rate at the side wall only 1.88% larger than at the radial centerline. As albedo decreases, and absorption becomes more dominant, the energy absorption at the side wall increases when compared to that at the centerline, with the difference between side wall and centerline energy absorption rate reaching a maximum of 24.1% for $\omega = 0.68$.

For the optically thicker medium of Fig. 7(b), the results differ greatly. Near the side wall, the energy absorption rate is greatest for smaller scattering albedo, as it was for the thin medium. However, due to the thickness of the medium and

the lack of propagation of radiant energy, an opposite result is seen as the centerline is approached. Excluding the case where $\omega = 0.98$, increases in scattering albedo produce an increase in energy absorption rate at the radial centerline.

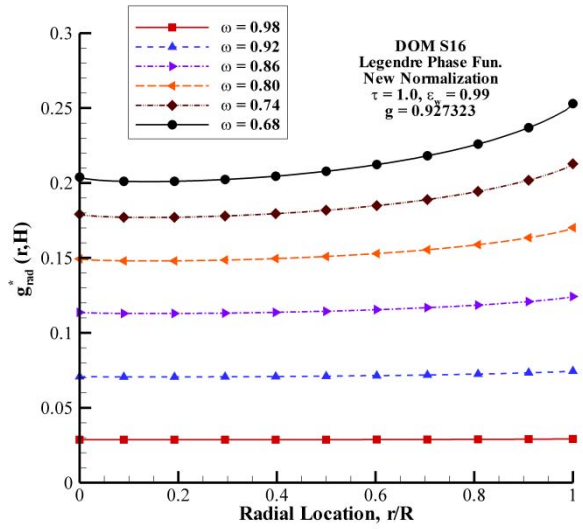

(a)

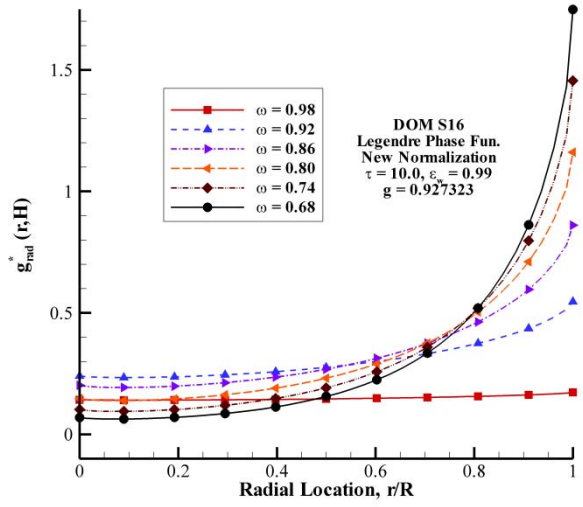

(b)

Figure 7: Volumetric radiative energy absorption rate vs. radial location for various scattering albedos with g = 0.927323 and a) τ = 1 and b) τ = 10

For the case where particle extinction is almost fully controlled by scattering ($\omega = 0.98$), the energy absorption rate is fairly constant over the entire absorber radius, with the ratio of energy absorption between the side wall and the radial centerline only reaching 1.22. This is due to the fact that the energy absorption rate depends directly on $(1 - \omega)$, so as the problem approaches pure scattering, the amount of energy absorption is vastly reduced and the impact of radial location becomes minimal (conforming to the results seen in Fig. 7(a) for the same scattering albedo). As scattering albedo decreases, the location along the absorber tube radius becomes substantial, with the ratio of energy absorption rate between the side wall and radial centerline reaching a maximum of 25.4 for $\omega = 0.68$. The differences in results between Figs. 7(a-b) indicate that both the scattering albedo and optical thickness of the medium can have a major impact on the volumetric radiative energy absorption rate.

The final quantity examined in this parametric study was the emissivity of the side wall. Fig. (8) plots side wall heat flux versus asymmetry factor for various side wall emissivities. The side wall emissivity is ranged from 0.8 to 0.99. The optical thickness and scattering albedo of the medium are kept constant at $\tau = 10$ and $\omega = 0.92$.

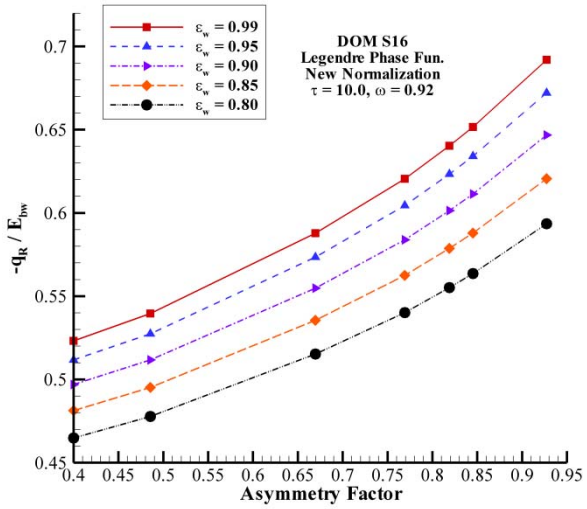

Figure 8: Side wall heat flux vs. asymmetry factor for varying side wall emissivity

As wall emissivity increases, the heat flux emanating from the side wall also increases due to the direct dependence of the side wall emissive power on the wall emissivity. Once again, as asymmetry factor increases, the heat flux is scattered more strongly away from the wall, leading to the witnessed increase in heat flux profile. The increase in heat flux with increasing wall emissivity becomes slightly more pronounced as asymmetry factor is increased. For example, the heat flux ratio between $\epsilon_w = 0.99$ and $\epsilon_w = 0.80$ is 1.13 for $g = 0.4$, 1.15 for $g = 0.7693$, and 1.17 for $g = 0.927323$.

Fig. (9) plots the volumetric radiative energy absorption rate vs. radial location for various asymmetry factors and wall emissivities. The energy absorption rate increases with

increasing wall emissivity, again due to the direct dependence of emissive power on wall emissivity. The optical thickness of the medium limits the propagation of radiant energy, leading to the opposite trends for varying asymmetry factor at the centerline and the side wall. As asymmetry factor increases, the difference in energy absorption rate between $\epsilon_w = 0.99$ and $\epsilon_w = 0.80$ increases. For $g = 0.4$, the energy absorption rate for $\epsilon_w = 0.99$ is 12.53% larger than the energy absorption rate for $\epsilon_w = 0.80$ for all radial locations, indicating that the impact of a change in wall emissivity is equal along the entire absorber tube radius. An increase in asymmetry factor to $g = 0.7693$ and $g = 0.927323$ increases the percent difference to 14.87% and 16.58%, respectively. These results show the importance of having a wall coating with a high emissivity in order to obtain the largest amount of energy absorption near the center of the solar absorber tube.

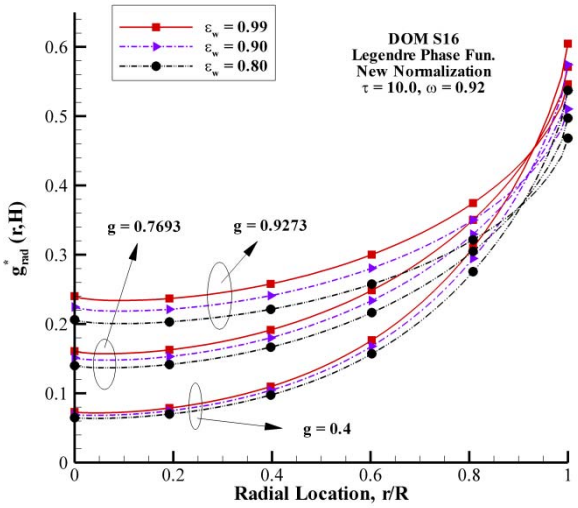

Figure 9: Volumetric radiative energy absorption rate vs. radial location for varying side wall emissivity

CONCLUSIONS

In this study, normalization of various phase functions was implemented in conjunction with the DOM to perform radiative transfer analysis inside a solar absorber tube. The following conclusions can be made based on this study:

(1) For cases where scattering is anisotropic, it is essential that the phase function normalization procedure conserves both scattered energy and asymmetry factor after directional discretization. The previously published technique of Kim and Lee [18] only considered conservation of scattered energy, and the lack of asymmetry factor conservation produced deviations in the phase function profile, and thus deviations in heat flux and energy absorption rate.

(2) When the new normalization procedure of Hunter and Guo [21,22] is implemented, asymmetry factor and scattered energy are exactly conserved regardless of whether the phase function is approximated using the Legendre or HG technique. In general, the lack of conservation of asymmetry factor inherent in the old technique produces larger changes in heat flux and energy absorption when the HG approximation is implemented as opposed to the Legendre approximation.

(3) For the HG approximation, errors in phase function value, heat flux, and energy absorption rate stemming from the lack of conservation of asymmetry factor with the old normalization strictly increase as asymmetry factor increases. For the Legendre approximation, the number of terms and shape of the phase function have a distinct impact on conservation after normalization. The largest errors in phase function values, heat flux, and energy absorption rate occur at g = 0.818923 with the Legendre approximation, as opposed to occurring at the highest g = 0.927323 with the HG approximation.

(4) Heat flux emanating from the side wall increases with increasing medium optical thickness and increasing wall emissivity, and decreases for increasing scattering albedo. Heat flux also increases with increases in asymmetry factor, due to the fact that energy is more strongly scattered away from the wall.

(5) Increases in optical thickness produce an increase in energy absorption rate near the side wall. For thinner media, where radiant energy is able to strongly propagate along the entire absorber radius, energy absorption rate at the centerline increases with increasing optical thickness. As the medium becomes thick, this trend reverses, and decreases in energy absorption at the centerline are witnessed due to the lack of radiant energy propagation. Increases in scattering albedo generally decrease the energy absorption rate at the radial centerline, and increases in wall emissivity uniformly increase the energy absorption rate along the entire absorber tube radius.

REFERENCES

[1] Modest, M.F., *Radiative Heat Transfer, 2nd ed.*, Academic Press, New York, 2003, pp. 263-284, 498-530.

[2] Siegel, R., Howell, J.P., *Thermal Radiation Heat Transfer, 4th ed.*, Taylor and Francis, New York, 2002, pp. 371-490.

[3] Webb, B.W., Viskanta, R., Analysis of heat transfer and solar radiation absorption in absorption in an irradiated thin, falling molten salt film, J. Solar Energy Eng., 1985, 107:113-119.

[4] Kim, K.H., Guo, Z., Multi-time-scale heat transfer modeling of turbid tissues exposed to short-pulsed irradiations, Computer Methods and Programs in Biomedicine, 2007, 86:112-123.

[5] Jiao, J., Guo, Z., Thermal interaction of short-pulsed laser focused beams with skin tissues, Physics in Medicine & Biology., 2009, 54:4225-4241.

[6] Carlson, B.G., Lathrop, K.D., Transport theory- the method of discrete-ordinates, in Greenspan, H., Kelber, C.N., Okrent, D. (eds.), *Computing Methods in Reactor Physics*, Gorden and Breach, New York, 1968.

[7] Fiveland, W.A., Discrete-ordinates solutions of the radiative transport equation for rectangular enclosures, Journal of Heat Transfer, 1984, 106:699-706.
[8] Fiveland, W.A., Discrete-ordinates methods for radiative heat transfer in isotropically and anisotropically scattering media, Journal of Heat Transfer, 1987, 109:809-812.
[9] Truelove, J.S., Three-dimensional radiation in absorbing-emitting-scattering media using the discrete ordinates approximation, Journal of Quantitative Spectroscopy and Radiative Transfer, 1988, 39:27-31.
[10] Menguc, M.P., Viskanta, R., Radiative transfer in axisymmetric, finite cylindrical enclosures, 1988, Journal of Heat Transfer, 108: 271-276.
[11] Jamaluddin, A.S., Smith, P.J., Predicting radiative transfer in axisymmetric cylindrical enclosures using the discrete ordinates method, Combustion Science and Technology., 1988, 62:173-186.
[12] Jendoubi, S., Lee, H.S., Kim, T.K., Discrete ordinates solutions for radiatively participating media in a cylindrical enclosure, Journal of Thermophysics and Heat Transfer, 1993, 7:213-219.
[13] Guo, Z., Kumar, S., Discrete-ordinates solution of short-pulsed laser transport in two-dimensional turbid media, Applied Optics, 2001, 40:3156-3163.
[14] Guo, Z., Kumar, S., Three-dimensional discrete ordinates method in transient radiative transfer, Journal of Thermophysics and Heat Transfer, 2002, 16:289-296.
[15] Kim, K.H., Guo, Z., Ultrafast radiation heat transfer in laser tissue welding and soldering, Numerical Heat Transfer A, 2004, 46:23-40.
[16] Jaunich M., Raje, S., Kim, K.H., Mitra, K., Guo, Z., Bio-heat transfer analysis during short pulse laser irradiation of tissues, Int. Journal of Heat and Mass Transfer, 2008, 51:5511-5521.
[17] Hunter, B., Guo, Z., Comparison of discrete-ordinates method and finite volume method for steady-state and ultrafast radiative transfer analysis in cylindrical coordinates, Num. Heat Transfer B, 2011, 59:339-359.
[18] Kim, T.K., Lee, H., Effect of anisotropic scattering on radiative heat transfer in two-dimensional rectangular enclosures, Int. Journal of Heat and Mass Transfer, 1988, 31:1711-1721.
[19] Wiscombe, W.J., On initialization, error and flux conservation in the doubling method, Journal of Quantitative Spectroscopy and Radiative Transfer,, 1976, 16:637-658.
[20] Boulet, P., Collin, A., Consalvi, J.L., On the finite volume method and the discrete ordinates method regarding radiative heat transfer in acute forward anisotropic scattering media, Journal of Quantitative Spectroscopy and Radiative Transfer, 2007, 104(1):460-473.
[21] Hunter, B., Guo, Z., Conservation of asymmetry factor in phase function normalization for radiative transfer analysis in anisotropic scattering media, Int. Journal of Heat and Mass Transfer, 2011, *submitted.*
[22] Hunter, B., Guo, Z., Phase Function Normalization for the Finite Volume Method in Radiative Transfer Analysis of Anisotropic Scattering Media, Int. Journal of Heat and Mass Transfer, 2011, *submitted.*
[23] Li, X., Weiqiang, K., Wang, Z., Chang, C., Bai, F., Thermal model and thermodynamic performance of molten salt cavity receiver, Renewable Energy, 2010, 35:981-988.
[24] Ghandehariun, S., Naterer, G.F., Dincer, I., Rosen, M.A., Solar thermochemical plant analysis for hydrogen production with the copper-chlorine cycle, Int. Journal of Hydrogen Energy., 2010, 35:8511-8520.
[25] Wang, F., Shuai, Y., Yuan, Y., Yang, G., Tan, H., Thermal stress analysis of eccentric tube receiver using concentrated solar radiation, Solar Energy, 2010, 84:1809-1815.
[26] Jianfeng, L., Jing, D., Jianping, Y., Heat transfer performance of an external receiver pipe under unilateral concentrated solar radiation, Solar Energy, 2010, 84 (11):1879-1887.
[27] Miri, R., Mraoui, S., Electrolyte process of hydrogen production by solar energy, Desalination, 2007, 206:69-77.
[28] Berman, A., Karn, R.K., Epstein, M., A new catalyst system for high-temperature solar reforming of methane, Energy & Fuels., 2006, 20:455-462.
[29] Rubin, R., Karni, J., Yeheskel, J., Chemical kinetics simulation of high temperature hydrocarbons reforming in a solar reactor, Journal of Solar Energy-Transactions of the ASME, 2004, 126:858-886.
[30] Rubin, R., Karni, J., Carbon dioxide reforming of methane in directly irradiated solar reactor with *Porcupine* absorber, Journal of Solar Energy-Transactions of the ASME, 2011, 133(2), 021008.
[31] Jiang, S., Hu, P., Mo, S., Chen, Z., Optical modeling for a two-stage parabolic trough concentrating photovoltaic/thermal system using spectral beam splitting technology, Solar Energy Materials & Solar Cells, 2010, 94:1686-1696.
[32] Karni, J., Kribus, A., Rubin, R., Doron, P., The 'Porcupine': a novel high-flux absorber for volumetric solar receivers, Journal of Solar Energy-Transactions of the ASME, 1998, 120: 85-95.
[33] Kim, T.K., Lee, H., Scaled isotropic results for two-dimensional anisotropic scattering media, Journal of Heat Transfer, 1990, 112:721-727.
[34] Lee, H., Buckius, R.O., Scaling anisotropic scattering in radiation heat transfer for a planar medium, Journal of Heat Transfer, 1982, 104:68-75.
[35] Vandenberghe, L., The QR Factorization, Class Lecture – Applied Numerical Computing EE1033, UCLA, 2011, http://www.ee.ucla.edu/~vandenbe/103/lectures/qr.pdf, accessed March 2011.
[36] Guo, Z., Maruyama, S., Scaling anisotropic scattering in radiative transfer in three-dimensional nonhomogeneous media, Int. Communications in Heat and Mass Transfer, 1999, 26:997-1007.
[37] Guo, Z., Kumar, S., Equivalent isotropic scattering formulation for transient short-pulse radiative transfer in anisotropic scattering planar media, Applied Optics, 1999, 39(24):4411-4417.